COBEM 2021 26th International Congress of Mechanical Engineering
November 22-26, 2021, Virtual Congress, Brazil

COB-2021-XXXX (XXXX is the identification number of the final paper)
On the use of PZT Transducers for Active Flutter Suppression

Frederico Albuquerque Ribeiro
Renan Sanches Geronel
São Paulo State University (UNESP), School of Engineering of Ilha Solteira, Ilha Solteira-SP Brazil
frederico.a.ribeiro@unesp.br,renan.sanches@unesp.br

Carlos de Marqui Junior
Department of Aeronautical Engineering, Sao Carlos School of Engineering, University of Sao Paulo, Sao Carlos, SP, Brazil
demarqui@sc.usp.br

Douglas D. Bueno
São Paulo State University (UNESP), School of Engineering of Ilha Solteira, Ilha Solteira-SP Brazil
douglas.bueno@unesp.br

Abstract. *The interest of this paper is to design a controller for an aeroelastic system using a piezoelectric actuator on a typical section model, investigating the actuator performance and limits. The aeroelastic model to be used is the typical section, using the Theodorsen unsteady aerodynamic loads, written in the time domain through rational function approximations (RFA). For the active suppression, an output feedback control is obtained using the Linear Matrix Inequalities (LMI) technique, with a piezoelectric actuator stack actuator. The piezoelectric stack is evaluated for flutter suppression. The electric voltage and power required to control the system are investigated by numerical simulation, preserving the actuator limits, the performance of the output feedback control for the time domain aeroelastic system (which contains non-measurable states, the lag states). Therefore obtaining the control laws, and the PZT actuator operation constraints, flutter suppression is achieved, improving the development and performance of the aeroelastic systems.*

Keywords: *aeroelasticity, aeroservoelasticity, Piezoelectric Stack, Active Flutter Suppression, Linear Matrix Inequalities, control*

1. INTRODUCTION

Flutter suppression is an important topic in aeroelasticity, due to the potentially catastrophic characteristics of this aeroelastic phenomenon, motivating continuous technological development on mitigating this undesirable instability. Due to advances of applied construction materials, such as reduction of the weight of aircraft, and a more flexible structure, the active controllers are strategies used not only to perform flutter suppression, but also allow the aircraft to operate on a larger flight envelope (which is composed by a higher height and velocities). In addition, these strategies are also desirable for unmanned aerial vehicles (UAV), operating in high-altitude long-endurance (HALE), which are very flexible vehicles designed to accomplish long-time flights without touching the ground. Several types of actuators can be employed for flutter suppression, and the piezoelectric actuators is a convenient alternative, since they do not require hydraulics systems to operate and these actuators class are briefly explored in the literature.

At the flutter condition, the structure exhibits oscillation amplitude that increases exponentially over time, leading it to collapse. Then, the engineering community has been developing strategies to lead with the flutter, and important techniques is active flutter suppression. Livne (2018) addressed the importance of using active controllers to suppress flutter. The author introduces that if used in the initial phases of the project, it can reduce the weight, increase of aircraft performance as well as assuring a positive impact on the build schedule and costs.

Several actuator types can be used to attenuate the flutter effect. The piezoelectric materials have been conquered significant importance in the mechanical systems, such as truss structures (Song *et al.*, 2001), helicopter rotor vibration suppression (Simões *et al.*, 2007). Sui *et al.* (2012) combined a vehicle engine frame with a stack piezoelectric actuator. This active control was used to reduce vibration in the system, present a low energy consumption, short response time, absence of dynamics components, and no need to use lubricants or other fluids. The piezoelectric stack actuator has been currently used in aeroelasticity due to its mechanical properties can be changed according to an electric current variation (Sihvola, 2007).

Nezami and Gholami (2015) study the use of piezoelectric material in active aeroelastic flutter characteristics and vibration control of supersonic honeycomb sandwich panels (in presence of elastic foundation). Numerical results shows

that the proposed controller is efficient in vibration and flutter suppression regardless the evaluated conditions (different layers, stiffness values). Silva and Carlos De Marqui (2017) investigate the use of piezoelectric materials as sensors and actuators in multilayered structures. Self-powered active vibration control is evaluated, in which one piezoelectric layer is used for scavenging energy, and the other is responsible for actuation control. To test the strategy effectiveness, a self-powered active controller is employed to damp the flutter oscillation of a plate-like wing. Therefore, flutter oscillations are successfully damped out when the proposed system is employed.

In this context, the main aim of this article is to evaluate the use of piezoelectric stack actuator to mitigate the flutter phenomena, considering the actuator operation characteristics, through a Linear Matrix Inequalities strategy to obtain the control. This paper also introduces an alternative model to couple the piezoelectric actuator adding one degree of freedom to simplify these coupling equations.

2. METHODOLOGY

The aeroelastic model is the typical section illustrated by the Fig. 1 with 4 degrees-of-freedom (DOF), with equation of motion given by Eq. 1, where $\mathbf{M}$ is the inertia matrix, $\mathbf{B}$ the damping matrix, $\mathbf{K}$ the stiffness matrix, $\mathbf{Q}$ the Theodorsen (1935) aerodynamic matrix, $q = \frac{1}{2}\rho V^2$ is the dynamic pressure and $\mathbf{u}(t) = \{h(t) \quad \theta(t) \quad \beta(t) \quad h_p(t)\}$ the displacement vector with plunge, pitch, control surface rotation and piezoelectric stack displacement. The fourth degree-of-freedom $h_p(t)$ was included with the purpose of simplify the coupling of the piezoelectric stack to the plunge spring based on couplings of Zanetti (2021) and Brennan *et al.* (2008), more details of including the extra DOF in the classical 3-DOF typical section are described in the Appendix A.

$$\mathbf{M}_a\ddot{\mathbf{u}}(t) + \mathbf{B}_a\dot{\mathbf{u}}(t) + \mathbf{K}_a\mathbf{u}(t) + q\sum_{j=1}^{n_{lag}}\mathbf{Q}_{j+2}u_{aj}(t) = \mathbf{B}_{pzt}\mathbf{u}_c(t) \tag{1}$$

where $\mathbf{M}_a = \mathbf{M} - q\frac{b^2}{V^2}\overline{\mathbf{Q}}_2$, $\mathbf{B}_a = \mathbf{B} - q\frac{b}{V}\overline{\mathbf{Q}}_1$ and $\mathbf{K}_a = \mathbf{K} - q\overline{\mathbf{Q}}_0$.

The aerodynamic matrix are obtained in the time domain through a rational function approximation, once that Theodorsen's aerodynamic coefficients are described in the reduced frequency. The Least Square method used are known as Roger's method (Roger, 1977; Abel, 1979), the Laplace domain rational function approximation is given by:

$$\mathbf{Q}(s) = \mathbf{Q}_0 + \mathbf{Q}_1 s\left(\frac{b}{V}\right) + \mathbf{Q}_2 s^2\left(\frac{b}{V}\right)^2 + \sum_{j=1}^{n_{lag}}\mathbf{Q}_{(j+2)}\left(\frac{s}{s+\frac{V}{b}\gamma_j}\right) \tag{2}$$

where the coefficients $\mathbf{Q}_n$ are calculated using the Least Squares, considering 7 lag parameters γ_j, chosen by an empirical equation ((Zona, 2011)) and based on the approximation accuracy demonstrated on (Ribeiro *et al.*, 2020). Then the aerodynamic matrices are obtained with 4 degrees of freedom in Eq. 12.

$$\gamma_j = 1,7k_{max}\left(\frac{j}{n_{lag}+1}\right)^2 \tag{3}$$

where, n_{lag} is the number of lag parameters and k_{max} the largest reduced frequency. Thereby the state-space system representation is given by:

$$\begin{cases}\dot{\mathbf{x}}(t) = \mathbf{A}\mathbf{x}(t) + \mathbf{B}_{oc}\mathbf{u}_c(t)\\ \mathbf{y}(t) = \mathbf{C}\mathbf{x}(t)\end{cases} \tag{4}$$

where $\mathbf{A}$ the aeroelastic dynamic matrix, $\mathbf{B}_c$ the control input matrix and $\mathbf{C}$ the output matrix, defined in the Appendix A.

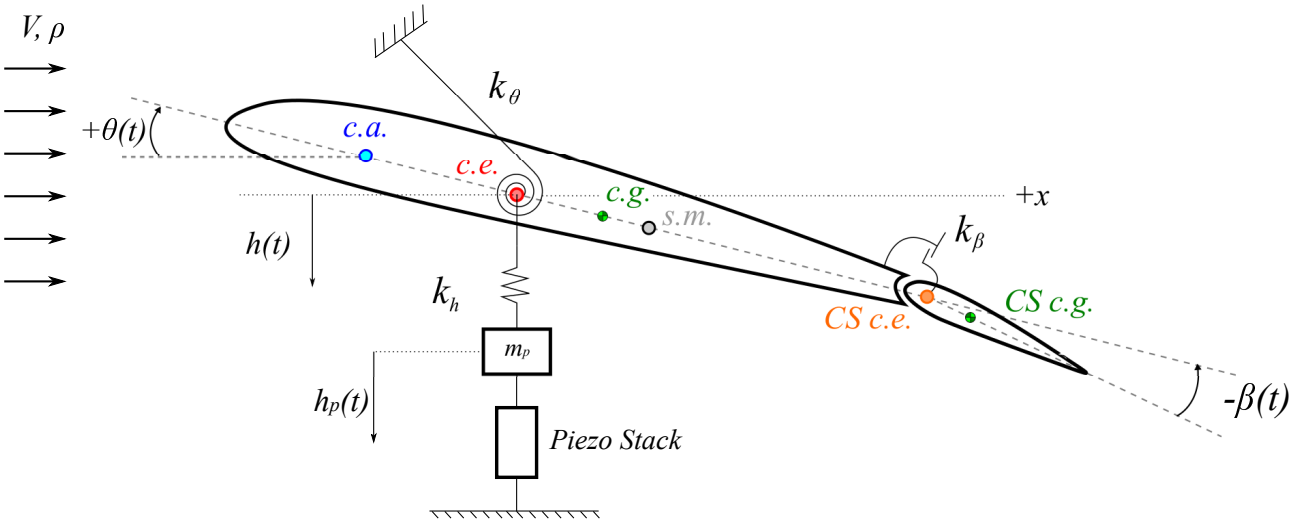

Figure 1. 4DOF typical section with piezoelectric actuator.

2.1 Piezoelectric Stack Actuator

Piezoelectric stacks are widely used in engineering applications because their size and ability to generate significant forces over small displacement range. Two strategies of piezoelectric stack as actuator are explored with small differences of the constitutive equations. The first approach considers a control using voltage applied on the stack and the other relies on the charge applied on the stack Main and Garcia (1997). Fig. 2 depicts the schematic illustration of a piezo stack.

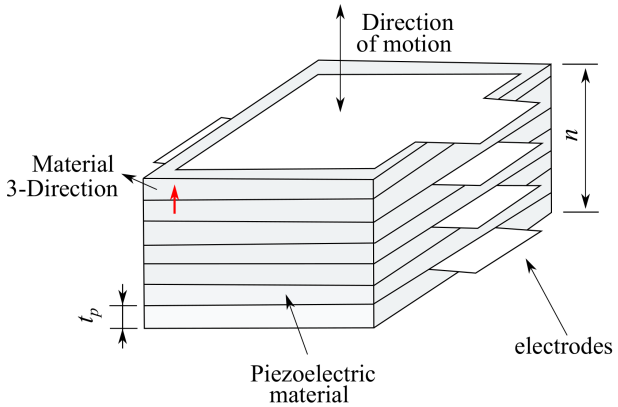

Figure 2. Schematic illustration of a piezoelectric stack actuator.

In this sense, the constitute relationship using charge control is defined as $T_3 = c_{33}^D S_3 - g_{33} c_{33}^D D_3$, where T_3 is the stress applied to the piezoelectric stack, c_{33}^D is the modulus at constant electric displacement, S_3 is the strain in the piezoelectric material, g_{33} is the piezo constant, and D_3 is the electric displacement. It is assumed that the actuator has a homogeneous geometry, assuring the stresses and fields to be limited to the 3 direction, the compression direction. Thereby, the electric displacement is represented by applying Gauss law for dielectrics, yielding $D_3 = Q_{in}/nA_{33}$, where Q_{in} is the charge applied to the stack, n is the number of stack layers, and A_{33} represents the stack cross-sectional area. Also, the strain in the piezoelectric material, considering the three directions can be expressed as $S_3 = h_p/nt_p$, where h_p is the actuator tip deflection, and t_p is the stack layer thickness. Combining the equations of T_3, D_3 and S_3 noticing that $T_3 = F/A_{33}$, the actuator force generated from the piezoelectric stack results in:

$$F_p = \frac{A_{33} c_{33}^D}{nt_p} h_p(t) - \frac{g_{33} c_{33}^D}{n} Q_{in}(t) \tag{5}$$

and represents the relationship for the charge-activated piezoelectric actuator. The charge applied to the piezoactuator can be rewritten as $Q_{in} = C_{ap} V_{in}(t)$, where C_{ap} is the series capacitance, and $V_{in}(t)$ denotes the amplifier input voltage. The equation of motion of mass and stack piezoelectric actuator is defined as:

$$m_p \ddot{h}_p(t) = -\frac{A c_{33}^D}{nt_p} h_p(t) + \frac{g_{33} c_{33}^D C_{ap}}{n} V_{in}(t) \tag{6}$$

where the first term on the right side represents the equivalent stiffness of the piezoelectric k_p and the second term defines the force applied on the system F_p. The simplified relationship is rewritten as:

$$m_p\ddot{h}_p(t) = k_p h_p(t) + F_p V_{in}(t) \tag{7}$$

Eq. 7 is coupled with the classical 3dof aeroelastic system as described in Appendix A, introducing the 4th degree-of-freedom and mass m_p, since it is more convenient than coupling a piezoelectric actuator and spring directly.

2.2 LMI output feedback control design

The control design developed by Dong and Yang (2013) is an output feedback LMI (Linear Matrix Inequalities). For the time domain aeroelastic system obtained trough the rational function approximation, the augmented states due to the lag parameters are not measurable, thus the output feedback allows to use only the measurable ones. Eq. 8 is the LMI, being $\mathbf{W} = \mathbf{P}^{-1}$, $\mathbf{G}$ and $\mathbf{L}$ the variables matrices and the scalar $\tau > 0$, usually chosen in the interval of $0 < \tau < 1$.

$$\begin{bmatrix} \mathbf{AW} + \mathbf{WA}^T + \mathbf{B}_{oc}\mathbf{LTC} + (\mathbf{B}_{oc}\mathbf{LTC})^T & * \\ \mathbf{CW} - \mathbf{GTC} + \tau\mathbf{L}^T\mathbf{G}^T & -\tau\mathbf{G} - \tau\mathbf{G}^T \end{bmatrix} < \mathbf{0} \tag{8}$$

where

$$\mathbf{T} = \begin{cases} \mathbf{I} \text{ if } \mathbf{C} \text{ is non full rank} \\ \text{otherwise} \quad \left(\mathbf{CC}^T\right)^{-1} \end{cases} \tag{9}$$

solving the LMI the controller gain is given $\mathbf{G}_c = \mathbf{LG}^{-1}$ and the system in Eq. 4 is stable in closed loop with $\mathbf{u}(t) = \mathbf{G}_c\mathbf{Cx}(t) = \mathbf{G}_c\mathbf{y}(t)$.

3. RESULTS AND DISCUSSION

The method to couple the piezoelectric actuator including an extra degree of freedom (related to the $h_p(t)$), must not affect the behaviour of the original system). In this case, to verify the equivalence in an aeroelastic perspective, Figure 3 shows the comparison of the Vgf diagram, in which no significant difference in terms of frequency is related. Therefore, the presence of the coupling does not change the aeroelastic behavior, where both flutter velocities occur at $V_f = 18.7$ m/s.

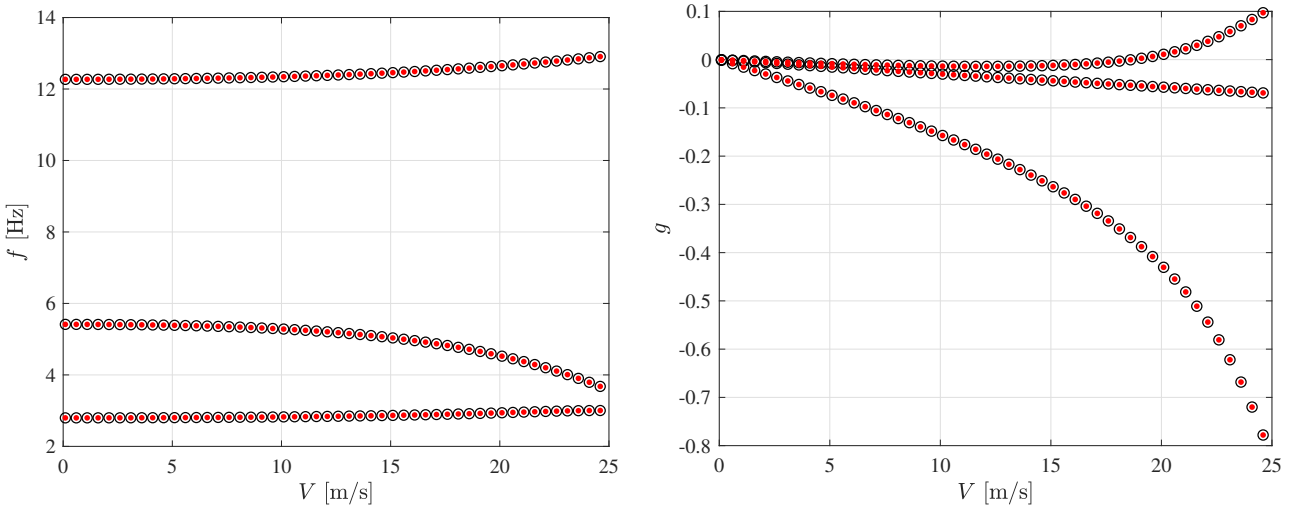

(a) V-f diagram (b) V-g diagram

Figure 3. Vgf comparison classical 3dof (•) model with 4dof (◯).

The eigenvalue of the 3dof system with $V = 0$ correspond to the frequencies 2.8 Hz, 5.5 Hz and 12.3 Hz, while for the 4dof system, 2.8 Hz, 5.5 Hz, 12.3 Hz and 11937 Hz, where this last value is related to the coupling mass and actuator stiffness. In practice, the approach used herein allows one to keep the typical section dynamics.

Table 1. Typical section airfoil physical and geometric properties.

Parameter	Value
airfoil semi-chord	$b = 0.15$ m
airfoil mass	$m = 5kg$
plunge frequency	$f_h = 3$ Hz
pitch frequency	$f_\theta = 4.5$ Hz
surface control frequency	$f_\beta = 12$ Hz
c.e measured from s.m	$a = -0.4$
location of CS c.e measured from s.m	$c = 0.6$
c.g from c.g	$x_\theta = 0.2$
CS c.g coordinate from c.e	$x_\beta = 0.0125$
radius of gyration of the airfoil referred to a a	$r = (0.25)^{1/2}$
radius of gyration of the CS referred to the hinge a	$r = (0.00625)^{1/2}$
air density	$\rho = 1.225$ kg/m^3
degrees of freedom	$dof = 4$

Table 2. Piezoelectric actuator properties.

Parameter	Value
Number of layers n	800
Cross-sectional area A_{33}	1×10^{-4} m^2
Layer thickness t_p	100×10^{-6} m
d_{33}	425×10^{-12} m/V
g_{33}	23.3×10^{-3} Vm/N
c_{33}^D	4.5×10^{10} Pa
C_ap	5 μF
m_p	0.01 kg

Figures 4 to 7 are the time domain response obtained using the airfoil properties disposed in the Tab. 1, and for the piezoelectric stack actuator in Tab. 2. Figure 4 depicts the plunge, pitch and control surface displacements and rotations comparison in presence and absence of the piezoelectric actuator, considering $V = 12$ m/s (velocity under flutter condition). The stack piezoelectric actuator demonstrates the capability of reducing the necessary time to the system achieve the equilibrium condition.

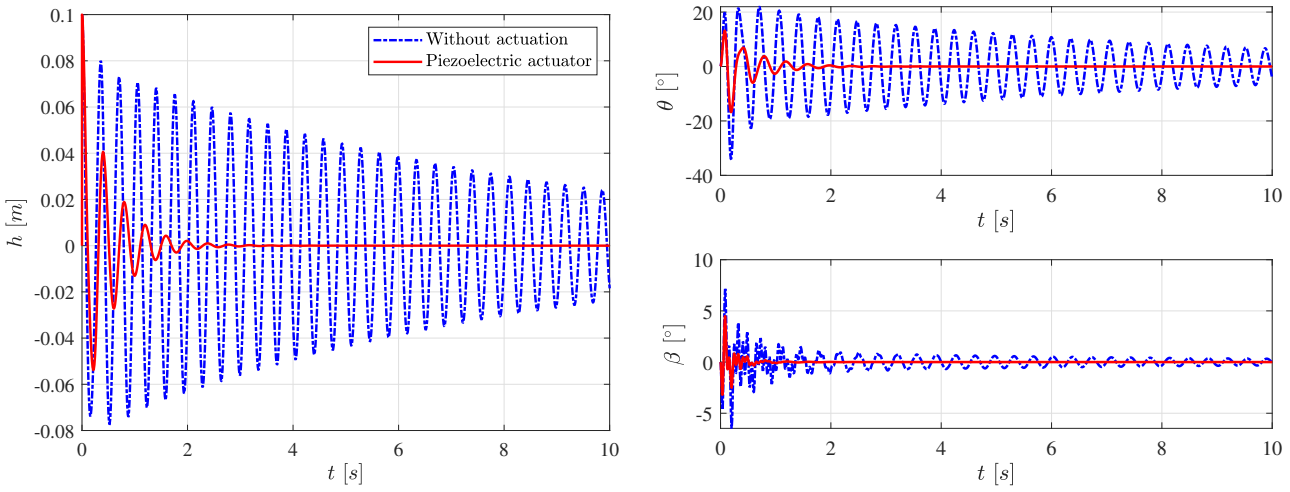

(a) Plunge displacement $h(t)$

(b) Pitch $\theta(t)$ and control surface rotation $\beta(t)$

Figure 4. Behaviour comparison in time domain of aeroelastic system with the actuator on and off, considering $V = 12$ m/s.

Figure 5 shows the stack actuator displacement, thought the mass m_p response, and the required voltage to control

the system. This actuator is based on that used by Ardelean *et al.* (2004, 2006), manufactured by NOLIAC in ceramic material, where the maximum operating voltage is 200 V and maximum stroke of 161 μm. Thereby this actuator can be used without damaging it.

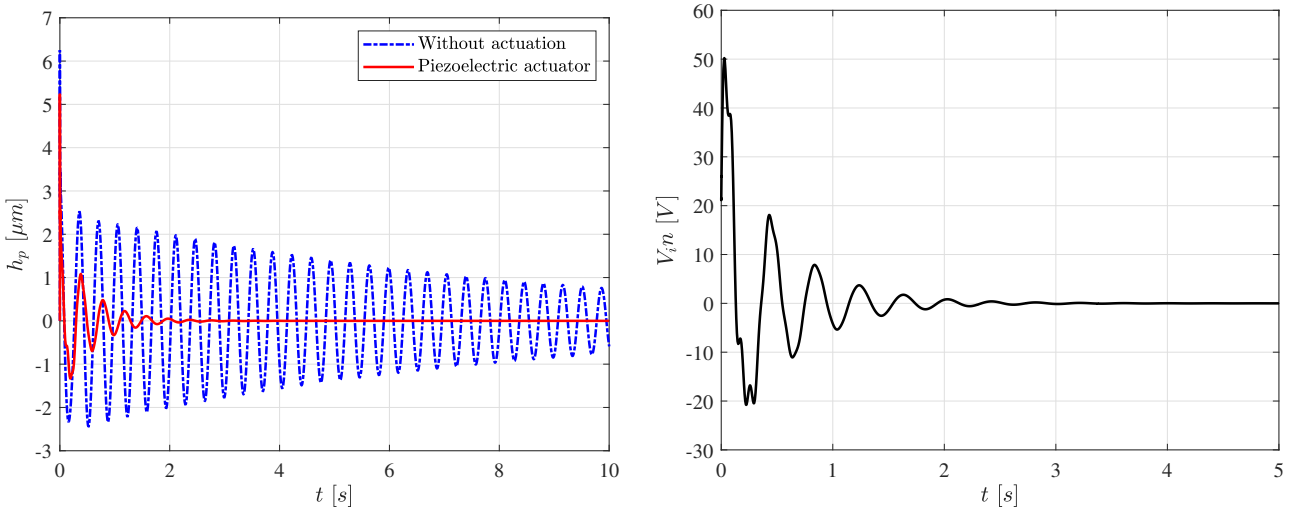

(a) Actuator displacement $h_p(t)$ (b) Input voltage V_{in}

Figure 5. Piezoelectric actuator response for $V = 12$ m/s

The case where $V = 20$ m/s represents the unstable region of Vgf diagram, and Fig. 6 shows the response comparison of the aeroelastic system behavior. The piezoelectric actuator has demonstrated the ability to stabilize the aeroelastic system, and the curves with the absence of the actuator illustrated the instability with exponential behavior of plunge, pitch, and control surface. Figure 7 shows that the actuator does not exceed the maximum operation inputs.

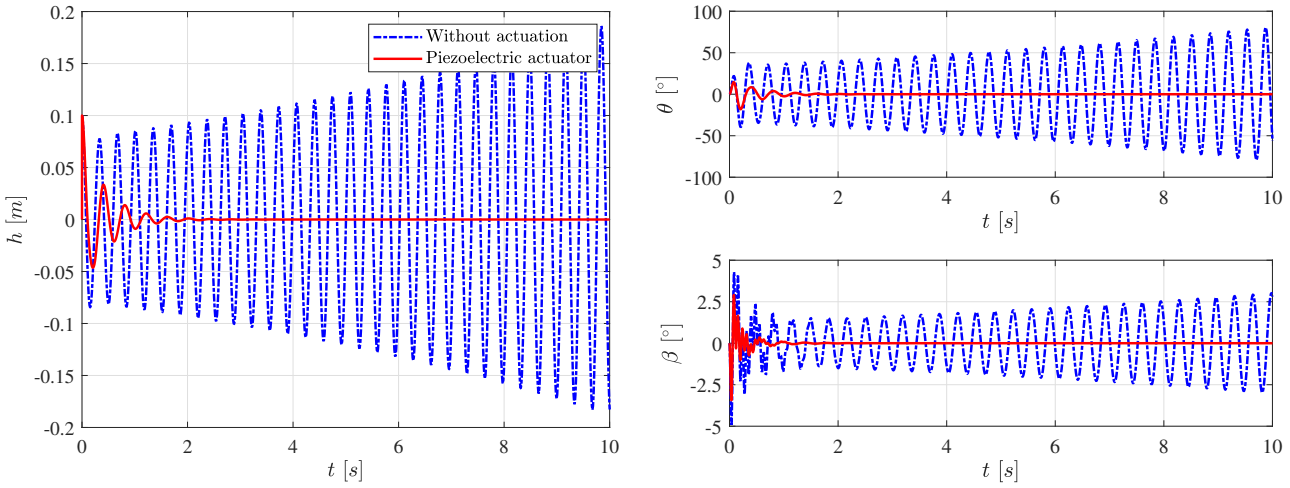

(a) Plunge displacement $h(t)$ (b) Pitch $\theta(t)$ and control surface rotation $\beta(t)$

Figure 6. Behaviour comparison in time domain of aeroelastic system with the actuator on and off, considering $V = 20$ m/s.

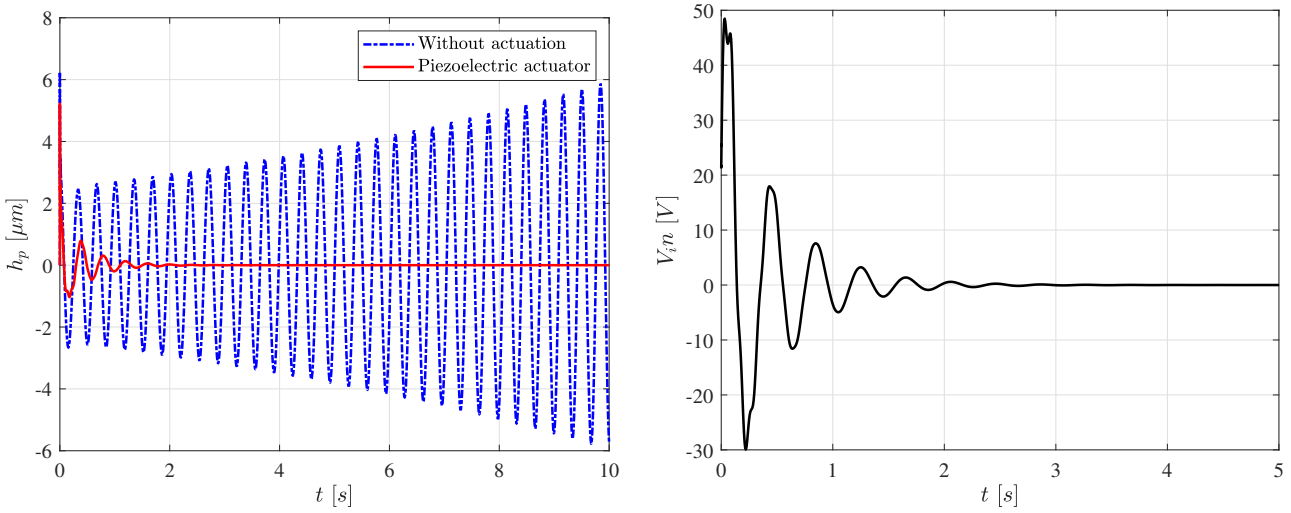

(a) Actuator displacement $h_p(t)$ (b) Input voltage V_{in}

Figure 7. Piezoelectric actuator response for $V = 20$ m/s

4. FINAL REMARKS

This paper evaluates the use of piezoelectric stack actuator to mitigate the unwanted oscillations. It is worth mentioning the presence of the proposed actuator does not change the system behavior, since its common eigenvalues and Vgf behavior are the same regardless of the presence of absence of the actuator on the system. A comparison of the aeroelastic dynamic behavior is presented for the presence and absence of the actuator, demonstrating that the actuator has the ability to stabilize the aeroelastic in a shorter time. Therefore, the coupling method of the actuator through the inclusion an extra degree of freedom does not influence on the aeroelastic behavior, as well simplify the coupled model as results in a faster response to reduce the instability of the system with a very low mass piezoelectric actuator.

5. ACKNOWLEDGEMENTS

This study was financially supported by the São Paulo Research Foundation (FAPESP; grant number 2019/24729-6) and the Coordenação de Aperfeiçoamento de Pessoal de Nível Superior - Brasil (CAPES) - Finance Code 001.

6. REFERENCES

Abel, I., 1979. "An analytical technique for predicting the characteristics of a flexible wing equipped with an active flutter-suppression system and comparison with wind-tunnel data". Technical report, National Aeronautics and Space Administration - NASA.

Ardelean, E.V., Cole, D.G. and Clark, R.L., 2004. "High performance ??v-stack??piezoelectric actuator". *Journal of intelligent material systems and structures*, Vol. 15, No. 11, pp. 879–889.

Ardelean, E.V., McEver, M.A., Cole, D.G. and Clark, R.L., 2006. "Active flutter control with a v-stack piezoelectric flap actuator". *Journal of Aircraft*, Vol. 43, No. 2, pp. 482–486.

Brennan, M., Carrella, A., Waters, T. and Lopes, V., 2008. "On the dynamic behaviour of a mass supported by a parallel combination of a spring and an elastically connected damper". *Journal of Sound and Vibration*, Vol. 309, No. 3, pp. 823–837. ISSN 0022-460X. doi:https://doi.org/10.1016/j.jsv.2007.07.074. URL https://www.sciencedirect.com/science/article/pii/S0022460X07006220.

Dong, J. and Yang, G.H., 2013. "Robust static output feedback control synthesis for linear continuous systems with polytopic uncertainties". *Automatica*, Vol. 49, No. 6, pp. 1821–1829. ISSN 0005-1098. doi:https://doi.org/10.1016/j.automatica.2013.02.047. URL https://www.sciencedirect.com/science/article/pii/S0005109813001362.

Livne, E., 2018. "Aircraft active flutter suppression: State of the art and technology maturation needs". *Journal of Aircraft*, Vol. 55, No. 1, pp. 410–452.

Main, J.A. and Garcia, E., 1997. "Piezoelectric stack actuators and control system design: Strategies and pitfalls". *Journal of Guidance, Control, and Dynamics*, Vol. 20, No. 3, pp. 479–485. doi:10.2514/2.4066. URL https://doi.org/10.2514/2.4066.

Nezami, M. and Gholami, B., 2015. "Active flutter control of a supersonic honeycomb sandwich beam resting on elastic foundation with piezoelectric sensor/actuator pair". *International Journal of Structural Stability and Dy-*

namics, Vol. 15, No. 03, p. 1450052. doi:10.1142/S0219455414500527. URL https://doi.org/10.1142/S0219455414500527.

Ribeiro, F.A., Dowell, E.H. and Bueno, D.D., 2020. "Enhancement to least square-based approach for time-domain unsteady aerodynamic approximation". *Journal of Aircraft*, Vol. 0, No. 0, pp. 1–14. doi:10.2514/1.C035824. URL https://doi.org/10.2514/1.C035824.

Roger, K., 1977. "Airplane math modeling methods for active control design." In *Structural Aspects of Active Control*.

Sihvola, A., 2007. "Metamaterials in electromagnetics". *Metamaterials*, Vol. 1, No. 1, pp. 2–11.

Silva, T.M.P. and Carlos De Marqui, J., 2017. "Self-powered active control of elastic and aeroelastic oscillations using piezoelectric material". *Journal of Intelligent Material Systems and Structures*, Vol. 28, No. 15, pp. 2023–2035. doi:10.1177/1045389X16685448. URL https://doi.org/10.1177/1045389X16685448.

Simões, R.C., Valder Steffen, J., Hagopian, J.D. and Mahfoud, J., 2007. "Modal active vibration control of a rotor using piezoelectric stack actuators". *Journal of Vibration and Control*, Vol. 13, No. 1, pp. 45–64. doi:10.1177/1077546306070227. URL https://doi.org/10.1177/1077546306070227.

Song, G., Vlattas, J., Johnson, S.E. and Agrawal, B.N., 2001. "Active vibration control of a space truss using a lead zirconate titanate stack actuator". *Proceedings of the Institution of Mechanical Engineers, Part G: Journal of Aerospace Engineering*, Vol. 215, No. 6, pp. 355–361. doi:10.1243/0954410011533356. URL https://doi.org/10.1243/0954410011533356.

Sui, L., Xiong, X. and Shi, G., 2012. "Piezoelectric actuator design and application on active vibration control". *Physics Procedia*, Vol. 25, pp. 1388 – 1396. ISSN 1875-3892. doi:https://doi.org/10.1016/j.phpro.2012.03.251. URL http://www.sciencedirect.com/science/article/pii/S1875389212006670. International Conference on Solid State Devices and Materials Science, April 1-2, 2012, Macao.

Theodorsen, T., 1935. "General theory of aerodynamic instability and the mechanism of flutter". Report 496, National Advisory Commitee for Aeronautics - NACA.

Zanetti, L.R., 2021. *Lumped Parameter and Modal Models to Simulate Ground Reaction Forces due to Running*. phdthesis, Unesp.

Zona, 2011. *ZAERO theoretical manual*. Zona Technology Inc., 02nd edition.

7. RESPONSIBILITY NOTICE

The author(s) is (are) solely responsible for the printed material included in this paper.

A STATE SPACE MATRICES

The extra degree of freedom in the system requires new matrices of the traditional 3DOF model. To couple the actuator and maintain the dynamical characteristics of the system, the coupling mass m_p must represent by lower values in comparison to the airfoil, and in this case $m_p = 0,02m$. The inertia matrix is obtained as follow:

$$\mathbf{M} = \begin{bmatrix} \mathbf{M}_{3dof} & \mathbf{0}^{3\times 1} \\ \mathbf{0}^{1\times 3} & m_p \end{bmatrix} \tag{10}$$

The stiffness,

$$\mathbf{K} = \begin{bmatrix} \mathbf{K}_{3dof} & \mathbf{K}_p^T \\ \mathbf{K}_p & k_p \end{bmatrix} \tag{11}$$

where $\mathbf{K}_p = \begin{bmatrix} -k_p & 0 & 0 \end{bmatrix}$.The piezoelectric actuator and the coupling mass have no interaction with the aerodynamics. Then the aerodynamic matrix must receive the last row and column with zeros, as follow,

$$\overline{\mathbf{Q}}_n = \begin{bmatrix} \mathbf{Q}_n & \mathbf{0}^{3\times 1} \\ \mathbf{0}^{1\times 3} & 0 \end{bmatrix} \tag{12}$$

where $n = 0, 1, \ldots, 2 + n_{lag}$, and the matrix $\mathbf{Q}_n$ is defined in Eq. 2. The aeroelastic dynamic matrix of the system $\mathbf{A}$ with the augmented states is given by:

$$\mathbf{A} = \begin{bmatrix} -\mathbf{M}_a\mathbf{B}_a & -\mathbf{M}_a\mathbf{K}_a & q\overline{\mathbf{Q}}_3 & \cdots & q\overline{\mathbf{Q}}_{2+n_{lag}} \\ \mathbf{I} & \mathbf{0} & \mathbf{0} & \cdots & \mathbf{0} \\ \mathbf{I} & \mathbf{0} & -\frac{V}{b}\gamma_1\mathbf{I} & \cdots & \mathbf{0} \\ \vdots & \vdots & \mathbf{0} & \ddots & \cdots \\ \mathbf{I} & \mathbf{0} & \vdots & \cdots & -\frac{V}{b}\gamma_{n_{lag}}\mathbf{I} \end{bmatrix} \tag{13}$$

I the identity matrix, and **0** is a zeros matrix. The matrices of the PZT actuator are represented as:

$$\mathbf{B}_{pzt} = \begin{bmatrix} 0 & 0 & 0 & \frac{g_{33} c_{33}^{D} C_{ap}}{n} \end{bmatrix}^{T} \tag{14}$$

$$\mathbf{B}_{oc} = \begin{bmatrix} \mathbf{M}_{a}^{-1} \mathbf{B}_{pzt} & \mathbf{0}^{1 \times dof} & \mathbf{0}^{1 \times 4n_{lag}} \end{bmatrix}^{T} \tag{15}$$

$$\mathbf{C} = \begin{bmatrix} \mathbf{I}^{dof} & \mathbf{0}^{dof \times dof} & \mathbf{0}^{dof \times 4n_{lag}} \\ \mathbf{0}^{dof \times dof} & \mathbf{I}^{dof} & \mathbf{0}^{dof \times 4n_{lag}} \end{bmatrix} \tag{16}$$